Optical coherence tomography as a tracking device for OCT guided laser cochleostomy: algorithm and first results

Yaokun Zhang[1], Tom Pfeiffer[2], Jia Ding[1], Wolfgang Wieser[2], Marcel Weller[3], Robert Huber[2], Joerg Raczkowsky[1], Heinz Woern[1], Thomas Klenzner[3]

[1] Institute for Process Control and Robotics (IPR), Karlsruhe Institute for Technology, Karlsruhe, Germany
[2] Chair for BioMolecular Optics at the Ludwig-Maximilians-Universität München, München, Germany
[3] Department of Oto-Rhino-Laryngology, Düsseldorf University Hospital, Düsseldorf, Germany

contact: yaokun.zhang@kit.edu

Abstract:

Conventional optical tracking systems have accuracy on the scale of several hundred micrometers. This is insufficient for an optical coherence tomography (OCT) guided laser cochleostomy which requires a much higher accuracy. In this paper, we evaluate the use of OCT itself as a tracking device by locating artificial landmarks generated around the cochleostomy. The results of the first experiments indicate that it is possible to achieve a mean absolute error of ca. 30µm for a single landmark using the proposed algorithm. An even smaller error is expected when at least 3-4 landmarks are used for the 3D tracking. The algorithm can be also used for the calibration and registration between the OCT and the laser ablation systems.

Key Words: optical tracking, optical coherence tomography, laser cochleostomy, calibration

1 Problem

Cochleostomy is a vital step of cochlear implantation (CI) to create an insertion channel on the cochlea for the electrode array of the implant. The feasibility of using a pulsed CO_2-laser to ablate hard tissue has been proven during the last years [1-5]. It can therefore be used to perform the cochleostomy by ablating the insertion channel pulse for pulse directly (figure 1a). With an axial resolution on the micrometer scale [6], optical coherence tomography (OCT) is a promising candidate for monitoring the bottom of the drilled channel. Recent research and our own experiments have confirmed that OCT can penetrate more than half a millimeter into compact bone tissue [7,8] and visualize the structure of the inner ear beneath the bone surface [9-11], for example the boundary between the lining membrane and perilymph (figure 1b). The combination of these techniques results in a closed loop control by guiding the laser cochleostomy system using OCT, where the laser ablation pattern is planned online according to the position of detected critical structures and avoid injury to them.

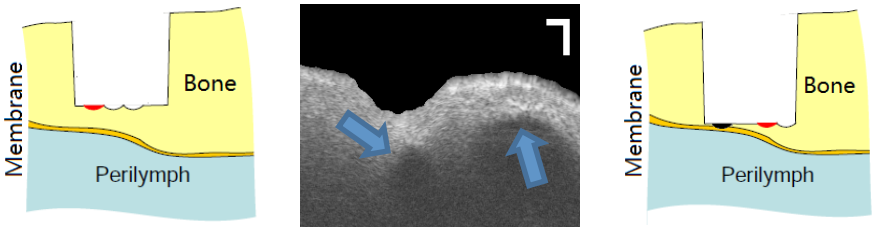

(a) (b) (c)

Figure 1 (a) Illustration of laser cochleostomy [5]. The diameter of the channel is ca. 1mm and the spot diameter is ~200µm; (b) an OCT B-Scan of a fresh pig cochlea during cochleostomy, in which the boundary between lining membrane and perilymph can be clearly seen. White bar = 250µm; (c) with tracking accuracy on the scale of several hundred micrometers, a planned pulse (red spot on the right) might be shot erroneously onto lining membrane (black spot on the left). Modified from [5].

After being navigated to an appropriate position, the laser system and patient should be fixed during the ablation process. Nevertheless, mechanical contact to the patient (e.g. squirting and aspirating water spray) or the laser system (e.g. switching to OP-microscope for a manual check of the cochleostomy) can easily cause a relative movement on the scale of hundred microns or even more. To ensure a maximum safety, the patient and laser system should be tracked.

Conventionally, a marker based optical tracking system, for example the NDI Polaris family, ARTTRACK etc., is considered to be the gold standard for such a case. Generally, these systems provide average accuracy of 0.25-0.3mm for

each tracked object. Considering the 200µm spot diameter of the CO_2 laser system we are using, this is already more than a whole spot off and in the worst case up to three times the spot size while tracking the patient and laser scanning optics simultaneously. This is critical because the laser pulse might be shot erroneously onto the lining membrane of sensible structures (e.g. the cochlea membranes) instead of the planned position on the remaining bone tissue (figure 1b). The distance between the marker and the cochleostomy would magnify the tracking error and make the situation worse.

Therefore, a more accurate tracking system is mandatory for our particular application. In this paper, we propose and evaluate the use of the OCT system itself as a tracking device with a much higher accuracy.

2 Methods

Eilers et. al. have proposed a highly accurate multimodal registration method between OCT and flat panel volume computerised tomography (fpVCT) based on comparing the internal structure of the scanned volume [12, 13]. In theory, the tracking during cochleostomy can be realized by the registration of two sequential OCT volumes applying this method. However, the cochlea consists of compact bone and is relatively homogenous without many internal structures. Moreover, storing and comparing the whole 3D volume is not efficient enough to achieve an acceptable tracking speed.

2.1 Tracking Concept

The idea to solve the above problems is simple: subsequent tracking only makes use of the 2D terrain information of the target surface obtained from the OCT data instead of the whole 3D volume. Furthermore, several artificial landmark holes are generated using either laser or burr around the cochleostomy (figure 2a) shortly before starting the ablation process. By locating and comparing the position of these landmarks instead of matching the whole surface, the channel can be tracked. The following criteria have to be satisfied while generating the landmarks:

1. No critical structures are injured.
2. The size of the holes is sufficiently large to be distinguished from roughness of the original surface.
3. The macroscopic curvature of the original surface should not be very large.

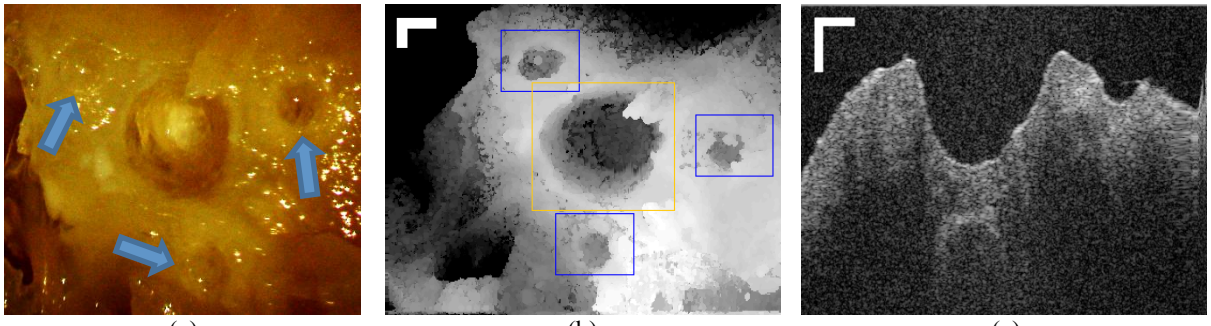

(a) (b) (c)

Figure 2 (a) OP-microscope image of the artificial landmarks drilled around the cochleostomy on a human cochlea with diameters of ca. 500µm; (b) the region of interest (yellow grid in the center) that covers the cochleostomy and the search range of the landmarks (blue grids) under OCT (en face mode); (c) an OCT B-Scan showing the cochleostomy and the landmark hole on the right of the cochleostomy in (a) and (b). White bars = 500µm in the air.

It is further assumed that the movement of the patient is limited to the millimeter range. Given a maximum possible displacement of the patient during each tracking loop, a search range centered at the previous position of each landmark is determined individually (figure 2b). The OCT will only scan the search ranges of the landmarks to reduce the amount of data and computing time. In the next section, an appropriate algorithm calculates the position of each landmark within a given search range will be explained.

2.2 Landmark Locating Algorithm

The first step of locating the landmark is the segmentation of the surface within the search range. Known as “ultra sound with light” and measuring the intensity of light echo, OCT images always have stronger intensity on media boundaries while only noises can be measured in the air (figure 2c). Therefore, the most superficial air-bone interface can be easily detected by calculating the vertical gradient of the image and searching for the first position where the gradient exceeds some threshold. Being independent of each other, the different scales in transversal and axial direction in the OCT volume are adjusted in this step.

The position of the searched landmark is then defined as the centroid of all the surface vertices within its 2D boundary on the bone surface. Due to the criterion 3 in section 2.1, a plane can be fitted to the surface and subtracted from it, so that the surface is macroscopically leveled. The vertical coordinates of the surface are then regarded as gray value and normalized to the range from 0 to 255, which results in a gray scale top view image (figure 3a). The conventional boundary detection and pattern recognition algorithms can be now applied to this image.

By multiplying the first and second derivative of the gray value of each pixel, the position of all potential boundary pixels can be extracted [14]. From figure 2c can be concluded that the candidate boundary pixels of a landmark always have negative second derivatives. Eliminate the non-candidate ones and the resulting landmark boundary appears to be a quasi-circular object (figure 3b), whose radius R can be roughly estimated. A common method to determine the center of such an object is to calculate its cross correlation with a circular pattern having the same radius and search for the position with the maximal value [15]. Considering the non-regular boundary shape of the landmark partially covered by drilling debris (see figure 3a) and the estimated radius of the circular pattern, a ring-shaped tolerance range surrounding the resulting center is defined. Only the pixels within this range are considered to be valid boundary pixels (figure 3b).

An ellipse is then obtained using least square fitting to these pixels. A new ring shaped tolerance range surrounding the center of the resulting ellipse can be defined again. Repeat the ellipse fitting and redefinition of the tolerance range until the difference between the ellipse centers of two sequential iterations is smaller than a given threshold or the maximal iteration is reached. The ellipse obtained from the last iteration is finally regarded as the landmark boundary. Each surface vertex within this ellipse is given a weight based on the area of its adjacent surface polygons and the centroid can be then calculated (figure 3c).

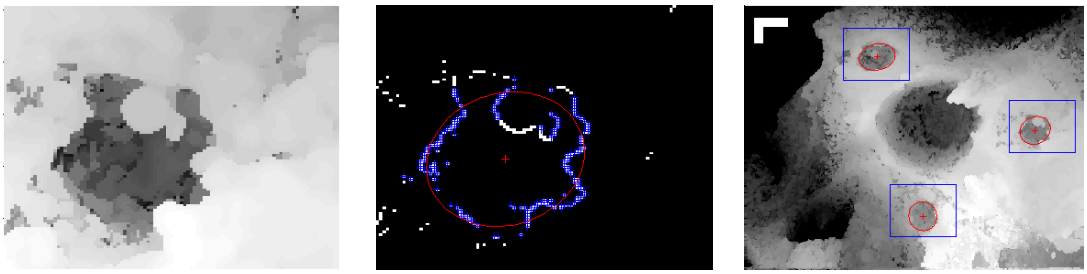

(a) (b) (c)

Figure 3 (a) gray value top view image of the landmark on the right of the cochleostomy in figure 2a and b; (b) extracted boundary pixels, detected center of the boundary (red cross in the middle), valid boundary pixels within the tolerance range (blue crosses) and ellipse fitted to the valid pixels; (c) results of the algorithm. White bar = 500µm.

3 Results

In figure 3c, the landmarks are precisely located on macroscopic scale. For a quantitative evaluation, two groups of experiments were conducted. For the first group, surface profiles of landmarks with different shapes (Gaussian and half sphere shaped) and incident angles were manually generated (figure 4a). The diameter and depth were 12 and 4 pixels respectively and their centroids were analytically calculated based on the geometry as reference results. For the second group, landmark craters were ablated using a single laser pulse on flat bovine bone specimen with a surrounding square shaped reference grid (figure 4b). The crater was ca. 130µm deep with a diameter of ca. 200µm and located exactly at the center of the grid. Two specimens with manually polished surface and original rough periosteum were prepared.

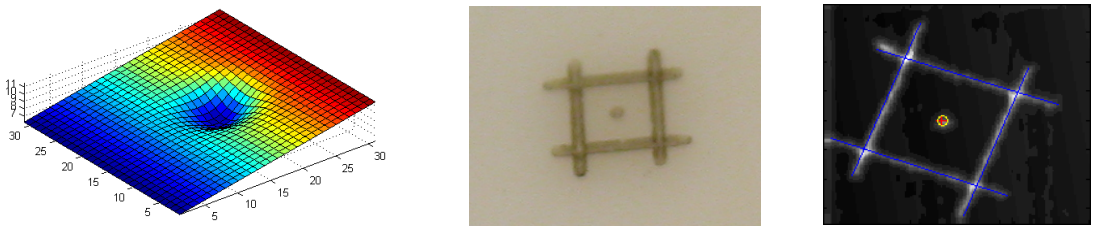

(a) (b) (c)

Figure 4 (a) a simulated Gaussian shaped test landmark with an incident angle of 10°; (b) a test landmark crater ablated at the center of a reference grid using a CO_2 laser; (c) the reference result (yellow circle) obtained by recognizing the grid using Hough transform (blue lines) and the result of the proposed algorithm (red cross).

After the detection of the four edges using Hough transform in the OCT images scanned with different incident angles, the center point of the grid on the original surface can be easily obtained. The offset from the surface to the centroid is calculated based on the 3D surface profile generated using a confocal microscope (NanoFoucs AG., Germany. Accuracy ~1µm). Subtracting this offset from the center of the reference grid, reference centroids are obtained (figure 4c).

For both groups, the stopping criterion of the iteration is set to 0.25 pixel size. The algorithm terminates after 2.89 iterations on average and maximal 5 iterations. The differences between the results of the algorithm and reference centroids are listed in table 1.

Table 1 difference and mean absolute error between the results of the algorithm and the reference centroids.

Group	shape/surface	0°	5°	10°	15°	20°	25°	30°	MAE
I [pixels]	Gaussian	0.73	0.73	0.81	0.62	0.52	0.60	0.66	0.67
	half sphere	0.23	0.27	0.36	0.37	0.55	0.55	0.48	0.40
II [µm]	polished	16.67	13.23	4.95	29.54	57.21	19.55	27.50	24.09
	periosteum	22.42	35.82	21.12	31.26	62.17	29.97	28.77	33.07

4 Disscussion

For the simulated landmarks, the mean absolute errors to the analytical reference centroids lie in sub-pixel range. The half sphere shaped landmarks with sharper boundary appear to have higher accuracy than the Gaussian shaped ones. For the real landmarks in the second group, the mean absolute error to the estimated reference centroids is around 30µm. The roughness of the original surface has slight negative influence on the accuracy. No dependency of the error on the incident angle can be concluded from either of the two groups. With these first results, we expect an even smaller global tracking error when at least 3-4 landmarks are used for the 3D tracking. It should be noticed that the current experiments are based on OCT data alone and an external reference system is required for the further evaluation of the tracking accuracy. Considering the demanding condition in the real surgery, for example landmarks partially covered by blood or ablation debris (figure 3a) etc., robustness tests and further improvements of the algorithm are necessary.

A sequential MATLAB version of the algorithm needs ca. 300ms for locating each landmark on an Intel Pentium Dual-Core E5300@2.6GHz with 2GB RAM Linux platform. Further optimization and parallelization of the algorithm is vital to achieve an acceptable tracking rate. Landmarks with different dimensions and specialized geometric shape can be easily ablated using the CO_2 laser system (figure 5a). By replacing the patterns used for the cross correlation and fitting, the algorithm can be easily adapted to the different landmark geometry. An optimal landmark size and shape regarding the accuracy and efficiency of the tracking will also be studied in the future work.

Being able to track the patient with extremely high precision, a calibration and registration between the OCT and laser ablation systems is still required, so that the ablation pattern planned in the OCT coordinate system can be precisely executed by the laser ablation system. This may also be done easily by ablating a calibration pattern shown in figure 5b and detecting the position of each crater using the proposed algorithm.

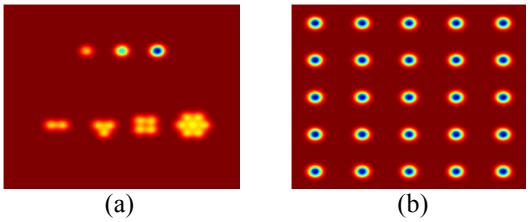

(a) (b)

Figure 5 Simulation of (a) landmark holes with different dimensions (first row) and geometric shapes (second row); (b) pattern for calibration and registration between OCT and laser ablation system.

Summarized, the proposed concept makes it possible to use OCT itself as a highly accurate tracking device during OCT guided laser cochleostomy without any additional hardware.

Acknowledgements

This research was sponsored by the German Research Foundation project OCT-LABS (DFG - WO720/25-1, KL2113/1-1, HU1006/2-1).

References

[1] M. Ivanenko, R. Sader, S. Afilal, M. Werner, M. Hartstock, C. Hänisch, S. Milz, W. Erhardt, H. Zeilhofer, P. Hering.: In vivo animal trials with a scanning CO2 laser osteotome, *Lasers in Surgery and Medicine*, Vol. 37, Issue 2, pp. 144–148, Aug. 2005.

[2] M. Frentzen, W. Götz, M. Ivanenko, S. Afilal, M. Werner and P. Hering.: Osteotomy with 80-µs CO2 laser pulses – histological results. *Lasers in Medical Science*, Vol. 18, Number 2 (2003), 119-124.

[3] Klenzner T, Knapp FB, Schipper J, Raczkowsky J, Woern H, Kahrs LA, Werner M, Hering P. High precision cochleostomy by use of a pulsed CO2 laser. *Cochlear Implants Int*. 2009;10 Suppl 1:58-62.

[4] Kahrs L.A., Burgner J., Klenzner T., Raczkowsky J., Schipper J., Woern H.: Planning and simulation of microsurgical laser bone ablation. *Int J. Comput. Assist. Radiol. Surg.,* Volume 5, Number 2 (2010), 155-162.

[5] L. A. Kahrs: *Bildverarbeitungsunterstützte Laserknochenablation am humanen Felsenbein*. KIT Scientific Publishing, 2009.

[6] Drexler, W., Fujimoto, J.G., Optical Coherence Tomograhpy, Springer, 2008.

[7] Ugryumova, Nadya; Matcher, Stephen J.; Attenburrow, Donald P.: Estimation of bone-mineral density from OCT image. *Proceedings of SPIE Volume* 5316, 128-135, 2004.

[8] B.Colston, U.Sathyam, L.DaSilva, M.Everett, P.Stroeve, L.Otis, "Dental OCT" *Opt. Express* 3, 230-238 (1998).

[9] Pau HW, Lankenau E, Just T, Hüttmann G..: Optical coherence tomography as an orientation guide in cochlear implant surgery? *Acta Otolaryngol.* 2007 Sep;127(9):907-13.

[10] Pau HW, Lankenau E, Just T, Hüttmann G..: Imaging of Cochlear Structures by Optical Coherence Tomography (OCT). *Laryngorhinootologie.* 2008 Sep;87(9):641-6. Epub 2008 Apr 17.

[11] Lin J, Staecker H, Jafri MS.: Optical coherence tomography imaging of the inner ear: a feasibility study with implications for cochlear implantation. *Ann Otol Rhinol Laryngol.* 2008 May;117(5):341-6.

[12] H. Eilers, M. Wienke, T. Ortmaier, O. Majdani, M. Leinung: Multimodal image registration of VCT and OCT images: a step towards high accuracy in surgical navigation. *Int J CARS* (2009) 4 (Suppl 1):S124–S133.

[13] J. Diaz Diaz, H. Eilers, A. Niemann, M. Leinung, O. Majdani, T. Ortmaier: Multimodale Bildregistrierung von fpVCT- und OCT-Daten zur Realisierung hochgenauer medizinischer Navigation. *CURAC*, 2010.

[14] R.Gonzalez, R.Woods: *Digital Image Processing*, 2nd edition, Publishing House of Electronics Industry, 2002.

[15] Marco Alexander Treiber: *An Introduction to Object Recognition.* Springer-Verlag London Limited 2010.